

# Flow through a hexagonal mixing grid with parabolic vanes measured experimentally by PIV in two planes at distances 1 and 5 × the maximum inscribed diameter D at Reynolds number based on D of $1.5 \cdot 10^4$ , $3.1 \cdot 10^4$ and $6.2 \cdot 10^4$

Václav Marek<sup>1</sup>, Anna Mrázová<sup>1</sup>, Vitalii Yanovych<sup>1</sup> and Daniel Duda<sup>1\*</sup>

<sup>1</sup>University of West Bohemia in Pilsen, Faculty of Mechanical Engineering, Department of Power System Engineering, Univerzitní 22, 306 14 Pilsen, Czech Republic

**Abstract.** Particle Image Velocimetry (PIV) method is used to measure the flow through a prototype mixing grid for nuclear reactor. In this preliminary experiment, there are no fuel rods, the grid is empty. We observe the pattern of jets and wakes, which is deformed by the transient flow introduced by the mixing vanes. The flow displays relatively low dependence on Reynolds number and high dependence on the downstream distance. In the contribution, there are shown the spatial maps of mean velocity, turbulence intensity and turbulence flatness.

## 1 Introduction

Many industrial applications need some mixing of fluids. It can be in order of both: to increase the heat transfer or to put the molecules of some reactants close. For this purpose, various systems are developed, e.g. the Taylor-Couette mixers (more details in [1], example of usage in [2]). The advantage of Taylor vortices is, that the mix even at laminar flow conditions and the critical velocity (expressed as Taylor number) is rather small to Taylor vortices to appear. Laminar flows can reasonably mix as well, see e.g. [3]. Another approach is to use a vibrating structure, which creates secondary stationary flow [4].

However, the best can be achieved by using fully turbulent flows, as the mixing is its natural feature. As stated in the article [5] “...*the grid turbulence offers a relatively low-pressure-loss possibility of intensifying mixing inside a channel (or pipe). On the other hand, the mixing scales are not distributed ideally – first in the near region of distinguished wakes and jets, there is intense mixing over small scales inside the wakes but the large-scale volumes stay separated; later, there are vortices larger than the mesh parameter  $M$ , which mix well the distant volumes, but the growing Kolmogorov scale leaves a gap between the smallest turbulent scale and the scale of molecular diffusivity.*”, see [5]. This issue can be partly solved by “infecting” the turbulence by a system of longitudinal vortices. Article [6] concludes that “(Past the swirler grid), the TKE displays delayed decay. This is similar

---

\* Corresponding author: [dudad@fst.zcu.cz](mailto:dudad@fst.zcu.cz)

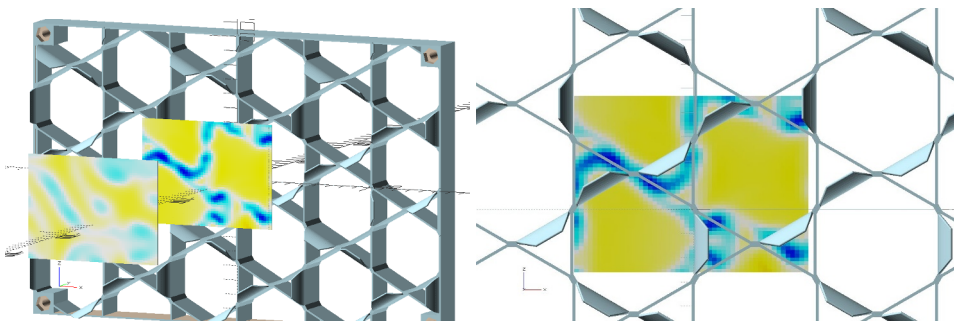
phenomenon like in the case of fractal grids [7], [8], [9], where the energy is injected at many length-scales; here the relatively stable stream-wise vortices smuggle the energy far downstream. Here is a possible practical application: maximum mixing is obtained not at the grid position, but more far downstream.”, see article [6]. It seems, that so-called “swirler grid” is the best. To be fair, we have to mention, that these longitudinal vortices come into the flow even by more natural phenomena: e.g. from the boundary layer [10] or as the secondary flow of second kind [11], which appear in turbomachinery as well [12], [13], where it is mostly unwanted.

This contribution shows the flow past a special grid developed by us. The motivation for creating this grid is to use it inside a nuclear reactor as a mixing grid [14]. Therefore, it has a hexagonal symmetry and it contains big holes for the nuclear fuel rods. Size of this hole  $D$  is used as the reference length-scale, while in the case of classical grid for turbulence research [15], the length-scale is the repeating periodicity  $M$  usually. This model grid is upscaled from the nuclear reactor scale by a factor of 5.49, thus the rod diameter  $D = 50.0$  mm and mesh parameter  $M = 67.033$  mm. If the reader is disappointed with the usage of  $D$  instead of  $M$ , he can multiply Reynolds number by a factor of 1.34 and divide the distances by this factor.

## 2 Experimental setup

The flow has been measured by using a standard method of Particle Image Velocimetry (PIV) [16], which is based on observing small particles carried by the flow and illuminated by a pulsed laser with two pulses separated by certain time-step  $\Delta T$ . The distance passed by the particles during this time is interpreted as the flow velocity, because the smaller the particles, the more relative importance of the surface forces acted by the surrounding fluid [17]. In contrast to other methods, PIV offers the direct insight into the structures of flow [18]. Our system consists of two cameras Flow Sense Mk II and solid-state laser New-wave Solo of energy of 500 mJ per pulse. Data processing is performed within the Dantec Dynamic Studio software.

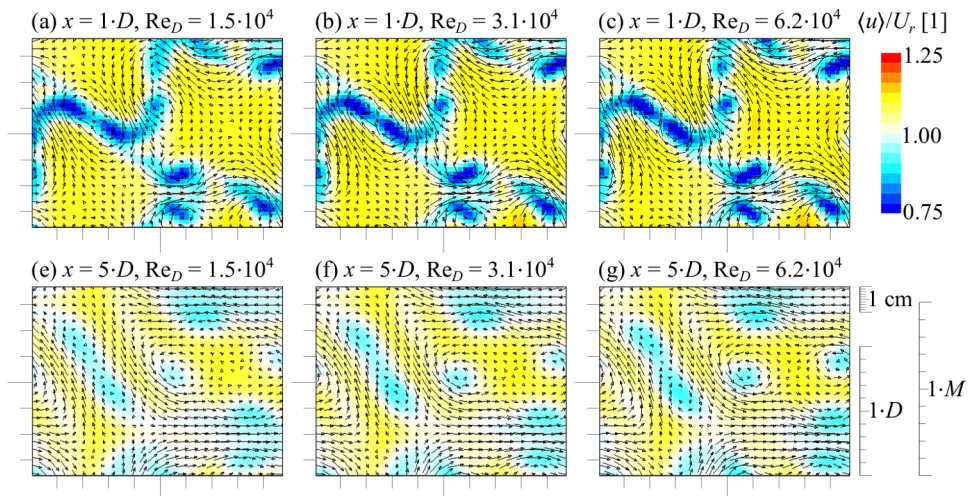
The explored grid is designed within the software OpenSCAD [19] and printed by using the Prusa Mk4 3D printer from polymerized lactic acid (PLA) [20]. It is placed in the transparent test section of the open low-speed aerodynamic tunnel at the University of West Bohemia in Pilsen. The cross-sectional size is  $20 \times 30$  cm<sup>2</sup>. The measured plane is located at the outlet of the test section and the distance past the grid is modulated by shifting the grid upstream.



**Fig. 1.** (a) The position of measured planes in respect to the grid. (b) placement of the Field of View (FoV) in respect to the grid. The colourscale represents the stream-wise velocity, see next figure for the values.

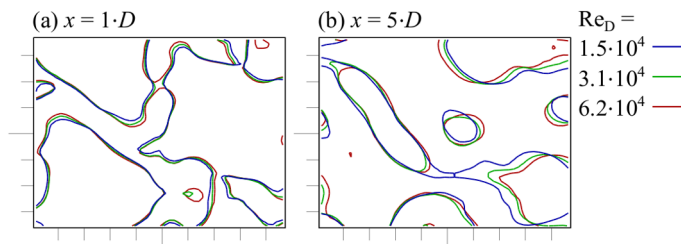
### 3 Results

Figure 1 shows the spatial map of ensemble average stream-wise velocity component denoted  $u$ . The other two components are represented using arrows. Only every second arrow is plotted for clearance. There can be seen the footprint of the grid structure deformed by the mixing vanes at smaller distance of 1 inscribed diameter  $D$ . Comparison of the measured area and the grid in stream-wise projection in Fig. 1b clearly shows their effect. The wake seems to be deepest at the location of shear areas between oppositely oriented vane-induced streams (at middle-left part of the FoV); while at the bottom-central part, there is a wake past single vane (there is no other vane in the direct neighbourhood, see Fig. 1b) and this wake is characterized by a pair of counter-rotating vortices. The effect of jet deflected by vane is observable even at neighbouring inter-vane shear layer: the top-right vane is outside of the FoV, but it destabilizes the wake past the top-central vane, which causes asymmetry of the middle-central vane wake.



**Fig. 2.** Ensemble average stream-wise velocity component  $u$  normalized by the wind tunnel velocity  $U_r$ , which ranges from 5 m/s to 20 m/s.

The flow in the more distant area, see Fig. 2efg, is less connectable with the grid structure. We can observe a long jets / wake structure in the central-left region and double weak vortices in the central-right area. At the bottom, there is observable a horizontal rightward jet, which can be associated with the isolated vane here.



**Fig. 3.** Comparison of the isotachs  $\langle u \rangle = U_r$  of the mean stream-wise velocity. Blue line refers to smallest velocity of 5 m/s, green to 10 m/s and red plays for 20 m/s.

The effect of Reynolds number seems to be small in the explored range (which is rather narrow spanning only values over the factor of 4). Figure 3 compares the isotachs of the mean stream-wise velocity on the level of  $\langle u \rangle = U_r$ . The effect of Reynolds number is slightly stronger downstream: the areas of lower velocity shifts more along the mean in-plane flow with increasing velocity (compare bottom-left and top-left structures in Fig. 3b and Fig.2efg). On the other hand, the location of the inter-vane shear layer is unaffected by Reynolds number as well as the location of the mentioned steady vortices in the middle area.

The turbulence intensity  $I_T$  is calculated by using the instantaneous velocity vectors  $\vec{u}(\vec{x}, t) = (u(\vec{x}, t), v(\vec{x}, t), w(\vec{x}, t))$  according to [21] as

$$I_T(\vec{x}) = \sqrt{\frac{(u(\vec{x}, t) - \langle u \rangle_t(\vec{x}))^2 + (v(\vec{x}, t) - \langle v \rangle_t(\vec{x}))^2 + (w(\vec{x}, t) - \langle w \rangle_t(\vec{x}))^2}{3(\langle u \rangle_t^2(\vec{x}) + \langle v \rangle_t^2(\vec{x}) + \langle w \rangle_t^2(\vec{x}))}} \quad (1)$$

Its spatial map is shown in Fig. 4. Note that due to normalization by velocity magnitude the value of  $I_T$  would be larger in areas of slower velocity even at the same values of fluctuations. Extremely, its value would diverge towards infinity at the areas of zero mean velocity, e.g. at the recirculation bubble [22]. Fortunately, this is not my case, here the measured area lies far enough to not be affected by recirculation bubble and all velocities are larger than zero.

In the near field (Fig. 4abc), the areas of higher turbulence correspond to that of lower mean velocity, i.e. to the wake structure. To make this observation clearer, there are plotted isotachs of mean stream-wise velocity corresponding to the incoming velocity. On the other hand, in the more distant area, one can observe strips of larger  $I_T$  in the slower area and another strip of larger  $I_T$  in the area, where the velocity is slightly slower than around, but definitely only weakly, while the level of turbulence is comparable, or even larger than in the neighbouring wake strip. Additionally, the discussed weak vortices are associated with turbulence intensity signal, although it is probably caused more by the vortex meandering than by the turbulence in its strict sense, as discussed in [6].

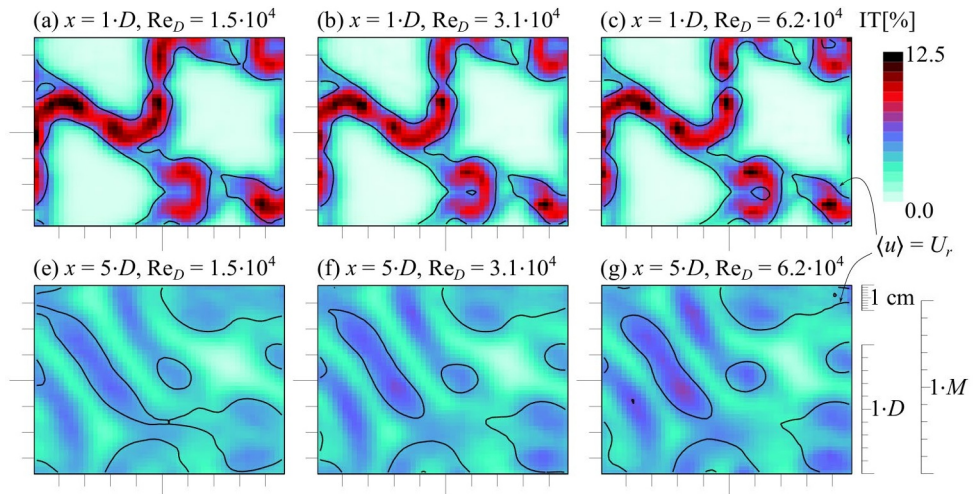


**Fig. 4.** Turbulence intensity. The black lines represents the isotachs of mean velocity.

Not only the level of fluctuation is important, but their length-scale as well. By using the Agrawal spatial decomposition [18] [23], the vector fields can be separated according to the length-scale of fluctuations. Three length-scale intervals has been selected and their TKE is calculated and combined by using three colour channels as described in the article [24] associating the red colour with the smallest fluctuations of size in the interval from 1.9 to 2.8 mm (i.e.  $(3.8 \cdot 10^{-2}D; 5.6 \cdot 10^{-2}D)$ ), the green color channel represents the fluctuations in

the size interval of (5.7 mm; 7.6 mm) = (0.11D; 0.15D) and the blue colour is associated with the large length-scale of (15.2 mm; 22.8 mm) = (0.3D; 0.45D). The combined spatial map is in Fig. 5, note that the colorized electronic version of this article is needed.

Length-scale dependent TKE in Fig. 5 shows that the near area is free from largest-scale fluctuations (they would not fit inside the wakes), the observed colours are predominantly green and yellow (sum of red and green) with redder spots in the shear areas between wakes past neighbouring oppositely oriented vanes. Note that these red spots are brighter at larger velocity, which is caused by the fact, that TKE decays from small scales and thus there is more small-scale fluctuations left at higher Re [25]. For this reason, the more distant area (Fig. 5efg) almost lack any red or yellow colour. The dominating tone is green with little of blue, whose length-scale can be associated with the meandering of the entire wake. Also note, that the jets (higher speed areas past the larger empty spaces in the grid) are clearly displayed as black spot in the near area, while in the distant area the turbulence-free spot is much smaller and irregular.

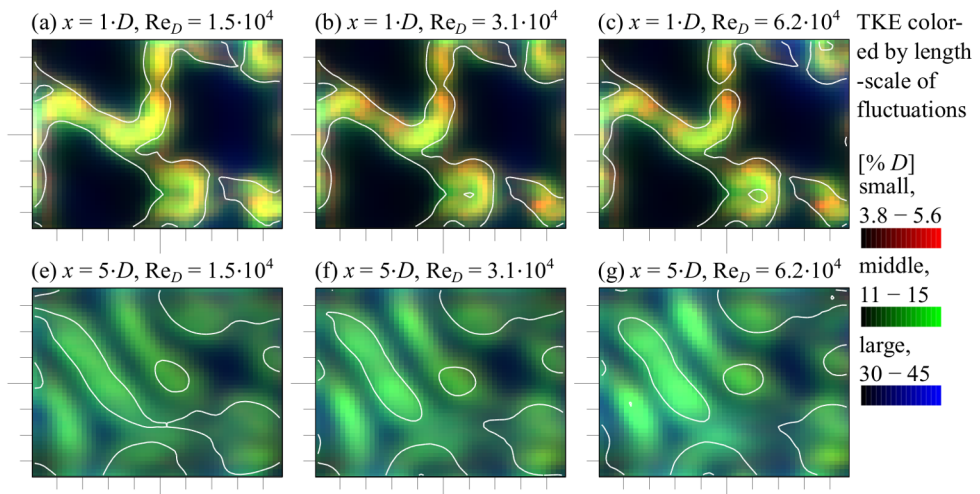


**Fig. 5.** Turbulent kinetic energy (TKE) coloured by the length-scale of contributing fluctuations. Large-scale fluctuations are plotted by using blue colour, middle-scale by green and small-scale fluctuations by red colour. The relative normalization between scales follow the Kolmogorov law [25] in a such way, that an ideal homogeneous turbulence would be plotted in grey. Note that the scaling between distances differs adapting to the actual strength, while that among Reynolds numbers keeps. The white lines show isotachs of mean velocity equal to input reference velocity  $U_r$ .

The distribution of velocity fluctuations typically follows the Gaussian distribution + so called “intermittency” [26], which is caused by short term switching the local flow into more or less turbulent state. As follows from the article [27], this effect takes place at the edge of turbulent wake, where the surrounding quieter fluid is time-to-time visited by more turbulent and slower fluid from the wake. Therefore, this feature can be used as a criterion for wake detection, because it offers sharper edge, than just a decrease of velocity. The intermittency effect is measured by using the *Flatness* [28], sometimes called *Kurtosis* or just *Fourth Statistical Moment*, in Czech *Koeficient špičatosti* (for the application for quantum turbulence see [29], [30])

$$F[u](\vec{x}) = \frac{\langle (u(\vec{x}, t) - \langle u \rangle_t(\vec{x}))^4 \rangle}{\langle (u(\vec{x}, t) - \langle u \rangle_t(\vec{x}))^2 \rangle^2} \quad (2)$$

The “neutral” value of this quantity is 3, because it is the value for Gaussian distribution. This can be proven analytically, but that is over the scope of this contribution. Larger  $F$  can

be interpreted as more often appearance of stronger events, while values smaller than 3 are typical for bounded probability (e.g. switching between two states, or the uniform distribution over a finite domain).

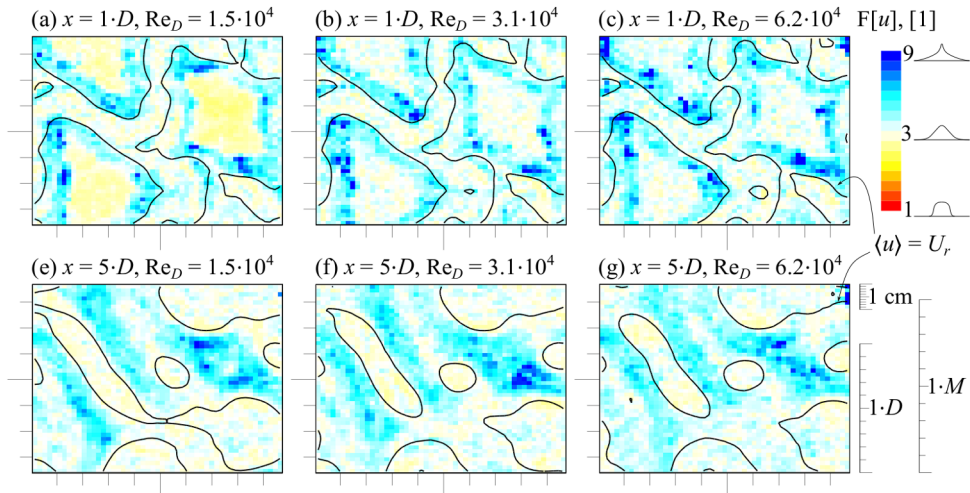


**Fig. 6.** Flatness, i.e. fourth statistical moment of the stream-wise velocity. The colorscale is in logarithmic scale. Note, that the value of 3 is flatness of Gaussian distribution.

Figure 6 shows, that the larger  $F$  is associated with the wake edge as predicted by [27], while the jet past the hole in the grid displays smaller values. This is strongly affected by Reynolds number, which can be caused by the stability of the wind tunnel, which is controlled via PID regulator based on dynamic pressure. As the measuring process produces a noise, and the pressure scales as  $p \sim U_r^2$ , then the *relative* noise level is much higher for lower velocities and the undisturbed velocity in the jet is like a random value from bounded range thus displaying low values of  $F$ .

At larger distances pas the grid, the high  $F$  areas focuses around the jet, while the wake spots display values gently smaller than 3.

## 4 Conclusion

This conference contribution describes the PIV measurement of the flow past a special grid. This grid has basically hexagonal symmetry as it was designed as mixing grid [14] for nuclear reactor. There are parabolic mixing vanes on some (not all) positions. These vanes eject the fluid forming jets not aligned with the main flow. These jets have a good potential to enhance mixing effect of this grid. In this contribution, we focused to the ensemble-averaged mean quantities in two distances past the grid. It is possible to distinguish clear structures coming from the wakes past vanes and from the shear layers between wakes past oppositely oriented vanes. The mean field displays weak vortices, which are probably caused by the tip-leakage flow on the edges of the mixing vanes, however, these vortices have not been analysed in this contribution of limited length, although we have an algorithm to do that [31].

## Acknowledgements

We acknowledge the support of the project SGS-2025-013 “Výzkum a vývoj moderních energetických strojů a zařízení”.

## Reference

- [1] M. Fardin, C. Perge a N. Taberlet, “The hydrogen atom of fluid dynamics” – introduction to the Taylor–Couette flow for soft matter scientists, *Soft Matter* **10**, 3523 (2014). <https://doi.org/10.1039/C3SM52828F>
- [2] O. Richter, H. Hoffman a B. Kraushaar-Czarnetski, Effect of the rotor shape on the mixing characteristics of a continuous flow Taylor-vortex reactor, *Chemical Engineering Science* **63**, 3504-3513 (2008). <https://doi.org/10.1016/j.ces.2008.04.003>
- [3] J. Fabisiak a S. Gepner, Quantification of laminar mixing efficiency with negative index Sobolev norm, *J. Phys.: Conf. Ser.* **2899**, 012005 (2024). <https://doi.org/10.1088/1742-6596/2899/1/012005>
- [4] D. Duda, P. Švančara, M. La Mantia, M. Rotter a L. Skrbek, Visualization of viscous and quantum flows of liquid He 4 due to an oscillating cylinder of rectangular cross section, *Phys. Rev. B* **92**, 064519 (2015). <https://doi.org/10.1103/PhysRevB.92.064519>
- [5] D. Duda, V. Yanovych a V. Uruba, An experimental study of turbulent mixing in channel flow past a grid, *Processes* **8**, 1-17 (2020). <https://doi.org/10.3390/pr8111355>
- [6] D. Duda a V. Yanovych, Interaction of stream-wise vortices generated by swirler grid, *Phys. Fluids* **36**, 055148 (2024). <https://doi.org/10.1063/5.0207124>
- [7] R. Gomes-Fernandes, B. Ganapathisubramani a J. Vassilicos, Particle image velocimetry study of fractal-generated turbulence, *JFM* **711**, 306-336 (2012). <https://doi.org/10.1017/jfm.2012.394>
- [8] D. Hurst a J. Vassilicos, Scalings and decay of fractal-generated turbulence, *Phys. Fluids* **19**, 3 (2007). <https://doi.org/10.1063/1.2676448>
- [9] P. Valente a J. Vassilicos, The decay of turbulence generated by a class of multiscale grids, *JFM* **687**, 300-340 (2011). <https://doi.org/10.1017/jfm.2011.353>
- [10] V. Yanovych, D. Duda, V. Uruba a P. Antoš, Anisotropy of turbulent flow behind an asymmetric airfoil, *SN Appl. Sci.* **3**, 885 (2021). <https://doi.org/10.1007/s42452-021-04872-2>
- [11] D. Duda, J. Bém, V. Yanovych, P. Pavlíček a V. Uruba, Secondary flow of second kind in a short channel observed by PIV, *Eur. J. Mech. B Fluids* **79**, 444-453 (2020). <https://doi.org/10.1016/j.euromechflu.2019.10.005>
- [12] D. Duda, M. Klimko, P. Milčák, M. Jeřábek, V. Uruba, V. Yanovych and P. Žitek, Wakes and secondary structures past stator wheel in test turbine VT-400 observed by PIV, *Eur. J. Mech. B Fluids* **105**, 151 - 163 (2024). <https://doi.org/10.1016/j.euromechflu.2024.01.008>
- [13] D. Duda, V. Yanovych, V. Uruba, Vortex profiles in grid turbulence observed by PIV, *AIP Conf. Proc.* **2672**, 020002 (2023). <https://doi.org/10.1063/5.0120078>
- [14] D. Duda, V. Yanovych a V. Uruba, PIV measurement of model nuclear fuel rod bundle, *J. Phys.: Conf. Ser.* **2899**, 012012 (2024). <https://doi.org/10.1088/1742-6596/2899/1/012012>
- [15] T. Kurian a J. H. M. Fransson, Grid-generated turbulence revisited, *Fluid Dyn. Res.* **41**, 021403 (2009). <https://doi.org/10.1088/0169-5983/41/2/021403>
- [16] R. J. Adrian, Twenty years of particle image velocimetry, *Exp. Fluids* **39**, 159-169 (2005). <https://doi.org/10.1007/s00348-005-0991-7>
- [17] C. Tropea, A. Yarin a J. Foss, *Springer Handbook of Experimental Fluid Mechanics*, (Berlin: Springer, 2007).

- [18] A. Agrawal a A. Prasad, Properties of vortices in the self-similar turbulent jet, *Exp. Fluids* **33**, 565–577 (2002). <https://doi.org/10.1007/s00348-002-0507-7>
- [19] Y. Lu, J. Ramos, D. Sarda, D. J. Shah, A. T. Becker a J. Leclerc, Open-Source CFD Simulation of Magnetic Rotating Swimmers with Experimental Validation, *IEEE International Conference on Automation Science and Engineering*, Bari, Italy, 3779-3784 (2024). <https://doi.org/10.1109/CASE59546.2024.10711422>
- [20] S. Inkinen, M. Hakkarainen, A. Albertsson a A. Södergard, From lactic acid to poly(lactic acid) (PLA): Characterization and analysis of PLA and Its precursors, *Biomacromolecules* **12**, 523-532 (2011). <https://doi.org/10.1021/bml01302t>
- [21] N. Basse, Turbulence Intensity and the Friction Factor for Smooth- and Rough-Wall Pipe Flow, *Fluids* **2**, 30 (2017). <https://doi.org/10.3390/fluids2020030>
- [22] D. Duda a V. Uruba, PIV of air flow over a step and discussion of fluctuation decompositions, *AIP Conf. Proc.* **2000**, 020005 (2018). <https://doi.org/10.1063/1.5049912>
- [23] A. Agrawal, Measurement of spectrum with particle image velocimetry, *Exp. Fluids* **39**, 836–840 (2005). <https://doi.org/10.1007/s00348-005-0018-4>
- [24] D. Duda a V. Uruba, Spatial spectrum from particle image velocimetry data, *ASME J of Nuclear Rad Sci.* **5**, 030912-1-030912-7 (2019). <https://doi.org/10.1115/1.4043319>
- [25] A. Н. Колмогоров, Локальная структура турбулентности в несжимаемой вязкой жидкости при очень больших числах Рейнольдса, *Воспроизводится по ДАН СССР* **30**, 299 (1941).
- [26] U. Frisch, *Turbulence: The Legacy of A. N. Kolmogorov*, (Cambridge: Cambridge University Press, 1995).
- [27] D. Duda, V. Uruba a V. Yanovych, Wake Width: Discussion of Several Methods How to Estimate It by Using Measured Experimental Data, *Energies* **14**, 4712 (2021). <https://doi.org/10.3390/en14154712>
- [28] P. Tabeling, G. Zocchi, F. Belin, J. Mauer a H. Willaime, Probability density functions, skewness, and flatness in large Reynolds number turbulence, *Phys. Rev. E* **53**, 1613-1621 (1996). <https://doi.org/10.1103/PhysRevE.53.1613>
- [29] M. La Mantia, P. Švančara, D. Duda a L. Skrbek, Small-scale universality of particle dynamics in quantum turbulence, *Phys. Rev. B* **94**, 184512 (2016). <https://doi.org/10.1103/PhysRevB.94.184512>
- [30] M. La Mantia, D. Duda, M. Rotter a L. Skrbek, Velocity statistics in quantum turbulence, *Procedia IUTAM* **9**, 79-85 (2013). <https://doi.org/10.1016/j.piutam.2013.09.008>
- [31] D. Duda, Searching of Individual Vortices in Experimental Data, *Vortex Dynamics - From Physical to Mathematical Aspects*, (London, IntechOpen, 2022.)